Surface plasma resonances in free metal clusters

Kathy Selby, Michael Vollmer,* Jun Masui,† Vitaly Kresin, Walt A. de Heer,‡ and W. D. Knight
Department of Physics, University of California, Berkeley, California 94720
(Received 13 March 1989)

Photoabsorption cross sections of small free neutral sodium clusters are measured in the wavelength range of 452–604 nm. The results indicate that the photoabsorption spectra are dominated by surface plasma oscillations of the valence electrons. The measured photoabsorption cross sections are consistent with a sum-rule calculation based on an ellipsoidal shell model and the experimental static electric polarizabilities of Na clusters. The calculated photoabsorption spectra of closed-shell clusters contain a single surface-plasma-resonance peak, whereas those of open-shell clusters have double or triple peaks. The experimental magnitudes of the photoabsorption cross sections near resonance peaks are between 1 and 2 Å^2 per delocalized electron.

I. INTRODUCTION

In this paper we describe the measurement of photoabsorption cross sections of free neutral sodium clusters containing $N=2-40$ atoms. First results of this work were discussed elsewhere;[1,2] here we give additional data and more details. We also present a model employed to predict the photoabsorption cross sections.

Optical spectroscopy is an essential tool for investigating the electronic properties of small metal clusters. Heretofore, it was carried out mainly for large clusters in matrices.[3,4] Extensive studies of surface-plasma-resonance absorption were made, but cluster-matrix interactions could not be eliminated, and the samples contained rather broad cluster-size distributions. Most data for alkali-metal clusters in beams also concerned large particles with broad size distributions,[5,6] or dimers and trimers.[7–9]

Recently, photoionization thresholds (for a review, see Ref. 10) and photoelectron spectra[11–13] of mass selected metal clusters have been measured. The data correlate well with the shell model for single-electron levels.[10,14,15] The photoabsorption experiments presented here demonstrate that in addition to single-particle excitations, collective electronic motion is also important, even for clusters containing fewer than eight delocalized electrons. Our results are consistent with predictions based on the measured static electric polarizabilities of Na clusters,[16,17] together with a shell model in which clusters are ellipsoidal in shape.

The plan of the paper is as follows. In Sec. II our apparatus configuration and data-taking procedures are outlined. In Sec. III we describe the mechanism by which clusters are removed from the beam following photon absorption. In Sec. IV we present a model for calculating the photoabsorption cross sections. In Sec. V we discuss our experimental data, and its relation to the simple ellipsoidal model and to some more elaborate theoretical calculations. Section VI contains our conclusions.

II. EXPERIMENTAL ARRANGEMENT AND MEASUREMENTS

The cluster-beam apparatus (see Fig. 1) is described in detail in Ref. 10. Neutral clusters are produced by super-

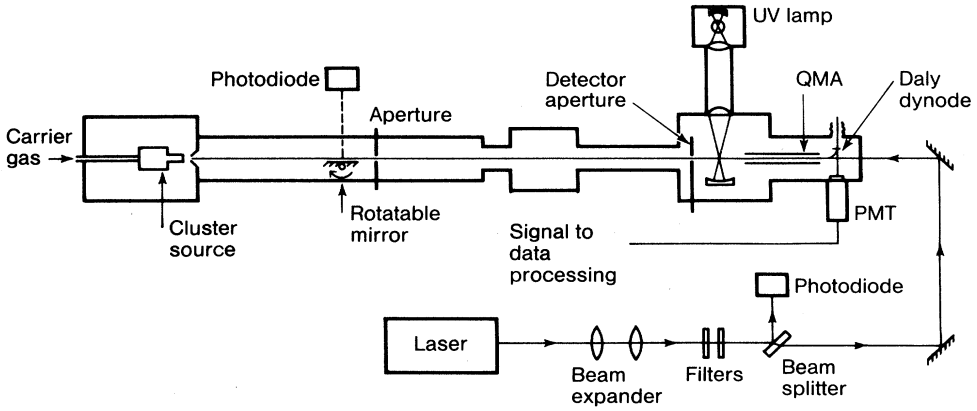

FIG. 1. Experimental configuration for the measurement of cluster photoabsorption cross sections. The cluster-beam source is operated at a Na vapor pressure of about 40 torr, with argon pressure of 300–500 kPa. The nozzle and skimmer have diameters of 0.0076 and 0.04 cm, respectively. A rectangular aperture (0.1×0.1 cm^2) is located 77 cm downstream; the detector aperture (0.2×0.3 cm^2) is located 2 m from the nozzle. The ionizing uv lamp is filtered; the filter has a transmission of $>5\%$ in the wavelength range 240–420 nm.

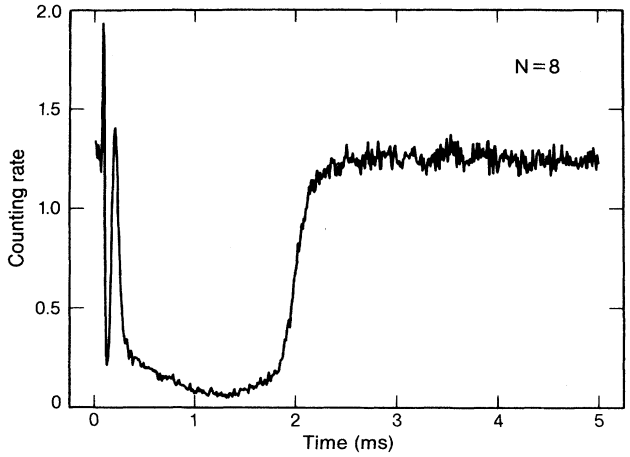

FIG. 2. Time-resolved scan for Na_8, showing the reduction in the cluster counting rate after illumination with the flashlamp laser. The laser pulses are 1 μs wide, and occur at time $t=90$ μs. The time resolution is 10 μs.

sonic expansion of sodium vapor and argon gas through a small nozzle. After passing through a skimmer, the cluster beam is collimated by a rectangular aperture. Further downstream, clusters pass through the detector aperture, and are then photoionized by uv light. The resulting ions enter a quadrupole mass analyzer (QMA), and the selected masses are steered into the detector.

The entire cluster beam is illuminated by a collinear and counterpropagating laser beam. A cw laser beam is chopped with an acousto-optic modulator; we used laser pulses of 100–350 μs width and a repetition rate of 100 Hz. The chopped beam is expanded to 0.6 cm diameter. An argon-ion laser is operated at selected wavelengths between 457.9 and 514.5 nm, with a bandwidth $\sim 3\times 10^{-3}$ nm. Near 560 and 600 nm, a cw dye laser with a bandwidth of 0.3 nm is used. The photon flux on the clusters is measured by rotating a mirror to intersect the laser beam, and the reflected light is directed onto a calibrated photodiode. The flight time of clusters from the source to the detector aperture is about 2 ms, which is much longer than the laser pulse width and much shorter than the time between consecutive pulses.

Some data were also taken using a flashlamp pumped pulsed dye laser, with a pulse width of 1 μs at a repetition rate of 10 Hz. This laser was operated near 450, 505, and 600 nm. Typical bandwidths were 0.5 nm.

One can adjust the QMA for a specific cluster mass and measure the counting rate of that cluster as a function of time after the laser pulse. The signals for many consecutive pulses are then summed. We call this a time-resolved scan (TRS), a typical example of which is shown in Fig. 2. For those clusters that were between the source and the detector aperture during a laser pulse, the counting rate is decreased, showing that interaction between photons and clusters removes some clusters from the beam.

During and shortly after the 1 μs wide laser pulses there is a large noise pulse (see Fig. 2), due to stray light entering the photomultiplier tube of the detector. This is followed by a depression more than 1 ms wide, which represents the cluster-beam depletion under the given experimental conditions, and defines a time window during which the counting rate is due only to clusters that were between the source and the detector aperture during the laser pulse. Finally, the signal returns to its undepleted value.

Most of our TRS data have used much longer laser pulses (100–350 μs width); these TRS's are very similar in appearance to Fig. 2. For a given wavelength and cluster size, the measured photoabsorption cross section (see below) is independent of the laser pulse width. At all investigated wavelengths, even at high light intensity, there is no depletion of the dimer signal. For all other investigated cluster sizes, laser powers of ~ 0.1 mJ/pulse produce substantial beam depletion.

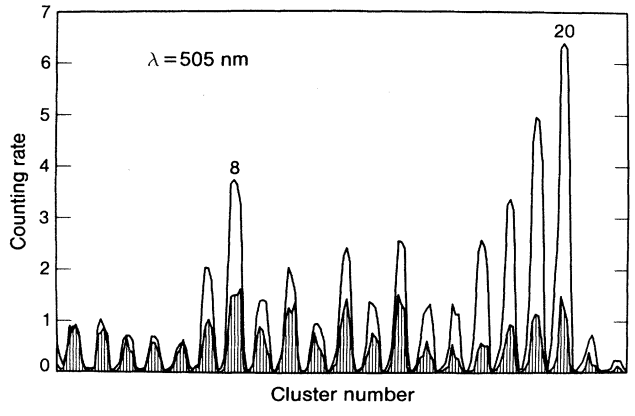

FIG. 3. Undepleted (light off) and depleted (shaded) mass spectra for Na_{2-21}. The depletion is caused by illumination of the cluster beam with laser light at 505 nm.

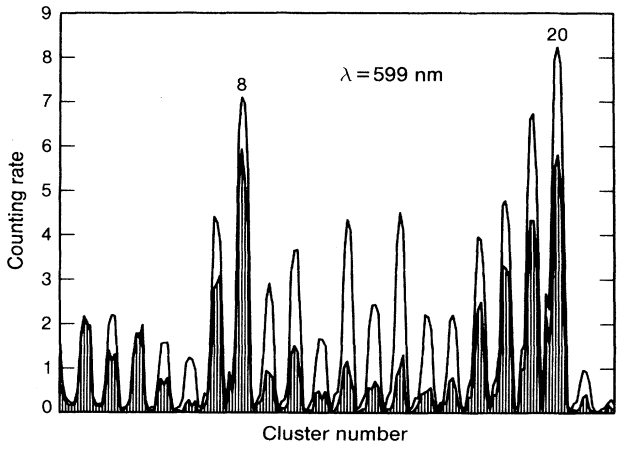

FIG. 4. Undepleted and depleted mass spectra for Na_{2-21}, with a laser wavelength of 599 nm.

Our measurements of photoabsorption cross sections are based on data taken in the form of gated mass scans (GMS's). For this mode of data collection, the QMA is adjusted to a specific mass and the counting rate in the time window described above is measured. Between consecutive laser pulses, the counting rate of unilluminated clusters is obtained. The QMA mass setting is increased and the counting rates are measured again. This process is repeated for a sequence of masses until the desired range of cluster sizes has been covered. More mass sweeps are added until the counting statistics are sufficiently good.

Figures 3 and 4 each show a GMS for Na_{2-21}, which were taken at wavelengths of 505 and 599 nm, respectively. The shaded signals show clusters which were illuminated but remained in the cluster beam, and thus reached the detector. The unshaded signals correspond to clusters which were not illuminated; they exhibit the well-known shell structure with spherical shell closings at $N=8$ and 20.[10] The ratio of depleted to undepleted counting rates (the "on/off ratio," r) in each mass peak, and the measured light intensity, are used to calculate the photoabsorption cross section for that cluster size (see Sec. III).

Within one GMS the light intensity is the same for all cluster sizes, but r is strongly size dependent. Comparison of Figs. 3 and 4 demonstrates that relative r values of different clusters depend on the laser wavelength. The cross section is therefore both size and wavelength dependent. Beam depletion was also observed for Na clusters as large as $N=59$, for K_{2-21}, and for mixed K-Na clusters. We note that soft ionization with properly filtered uv light, as employed in this apparatus, ionizes the jet cooled clusters without causing fragmentation.[17,18]

III. MECHANISM FOR BEAM DEPLETION

Absorbed photons excite surface plasma oscillations in a cluster (see Sec. IV), which then heats up, causing evaporation of atoms (or dimers). The transverse recoil of the daughter cluster removes it from the collimated beam. In the following, the photoabsorption cross sections will be expressed in terms of experimentally measured quantities, and the detection probability of daughter clusters will be discussed.

If single-photon absorption is sufficient to cause evaporation, then

$$\ln r = -\sigma\phi \ , \tag{1}$$

where r is the on/off ratio (see Sec. II), ϕ is the number of photons per unit area per laser pulse, and the constant of proportionality, σ, is the photoabsorption cross section. Figure 5 shows experimental values of $-\ln r$ versus ϕ for three selected clusters, based on data extracted from a series of GMS's. Least-squares fits to the data show that Eq. (1) is satisfied. This relationship between r and ϕ has been verified experimentally for clusters as large as $N=40$.

The evaporation rate of atoms after photon absorption is estimated in Appendix A; we find that evaporation occurs within a small fraction of the cluster flight time. The recoiling daughter cluster will not be detected unless

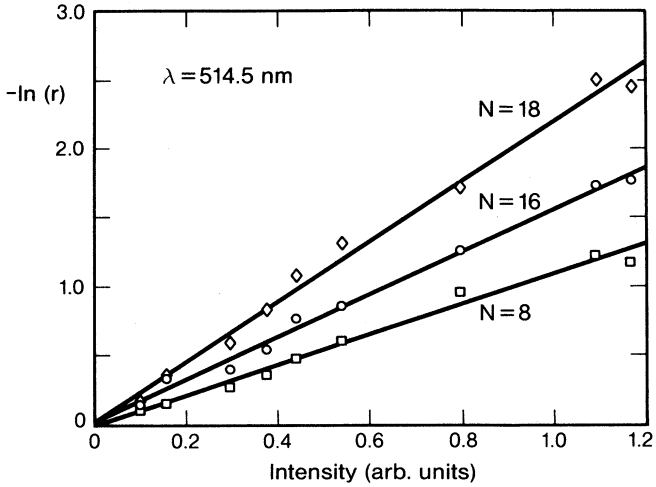

FIG. 5. Logarithm of the "on/off ratio," $-\ln(r)$, vs light intensity (arbitrary units) for Na_8 (squares), Na_{16} (circles), and Na_{18} (diamonds) at a wavelength of 514.5 nm. The solid lines are least-squares fits to the data.

it passes through the detector aperture; the detection probability, P_{det}, depends on the distance, L, between the cluster and the aperture at the time when evaporation occurs. P_{det} decreases rapidly as L increases (see Appendix B), because the daughters have more time to move in a transverse direction before crossing the plane of the aperture. For the experimental conditions of Fig. 2, P_{det} becomes negligibly small for $L \gtrsim 10$ cm. The rapid decrease of P_{det} with increasing L corresponds to the initial steep decrease in counting rate in Fig. 2.

In the region of greatest depletion in the TRS, a laser power of ~ 1 mJ/pulse is sufficient to reduce the counting rate to the background noise level for all cluster sizes investigated (except the dimer). This demonstrates experimentally that the daughter clusters are not detected. The gradual rise in the counting rate at the end of the signal depression is due to the spread in the cluster velocity distribution. Clusters which were formed after the laser pulse overtake slower illuminated clusters and reach the detector before them; the signal therefore shows less depletion. Quantitative analysis of the signal shape provides a simple technique for the measurement of velocity distributions of cluster beams.[19]

Some other examples of cluster photodissociation or desorption are mentioned here. In photodissociation experiments with Na_3, fluorescence from dissociated atoms was observed.[8] Beam depletion of sodium trimers due to photodissociation has been measured,[9] and the dissociated dimers were also detected. The wavelength ranges we have investigated are not sufficient to make a comparison between these data and our results, but there are some resemblances which encourage further measurements. Intense laser illumination of alkali clusters[20] causes successive rapid evaporation of neutral monomers. Experiments with sodium clusters of mean diameter 50 nm, adsorbed on a LiF(100) surface, suggest that laser excitation of surface plasma resonances causes nonthermal desorption of atoms from the clusters.[21]

IV. ELEMENTARY THEORY OF PHOTOABSORPTION CROSS SECTIONS

Our data show several indications that absorption of visible light causes excitation of surface plasma oscillations in metal clusters. The measured photoabsorption cross sections show resonances which have significantly more oscillator strength and lie at higher frequencies than is expected for the strongest single-electron excitations.[22] This suggests that a collective excitation is involved. The observed resonances are located close to several different theoretical predictions of the surface-plasma-resonance positions (see below). For open-shell clusters, the data are consistent with the predicted multiple surface-plasma-resonance peaks expected from nonspherical cluster shapes.

A. Spherical clusters

For spherical metal particles that are much smaller than the photon wavelength, classical Mie theory[23] provides the following expression for σ, the photoabsorption cross section:

$$\sigma=\frac{4\pi Ne^2}{m_e c}\frac{\omega^2\Gamma}{(\omega^2-\omega_0^2)^2+(\omega\Gamma)^2}\ , \tag{2}$$

where N is the number of valence electrons, ω_0 is the resonance frequency, and Γ represents the width of the resonance. Equation (2) assumes that all of the dipole oscillator strength is exhausted by the surface plasma resonance at ω_0 (the "surface-plasmon-pole approximation"[24]). In metal clusters this resonance is the collective oscillation of the valence electrons with respect to the positive ions.

Under the surface-plasmon-pole approximation, sum rules can easily be used to show (see, e.g., Ref. 25) that

$$\omega_0^2=\frac{Ne^2}{m_e\alpha}\ , \tag{3}$$

where α is the static electric polarizability of the cluster. For a classical monovalent metal sphere, $\alpha=Nr_s^3$, where r_s is the Wigner-Seitz radius of the metal. With $r_s=4.0$ a.u. for Na, the classical surface-plasma-resonance wavelength is 365 nm.

B. Ellipsoidal clusters

The polarizability of a metal ellipsoid has a different value, α_i, along each of the three principal axes, and the photoabsorption cross section depends on the orientation of the ellipsoid with respect to the photon polarization. For randomly oriented ellipsoidal clusters, the photoabsorption spectrum is the sum of three resonances of equal weight. Equation (2) can be generalized to give

$$\sigma=\frac{4\pi Ne^2}{3m_e c}\sum_{i=1}^{3}\frac{\omega^2\Gamma_i}{(\omega^2-\omega_{0i}^2)^2+(\omega\Gamma_i)^2}\ , \tag{4}$$

where the sum is over the three principal axes. The Γ_i represent the widths associated with each of the three resonances at ω_{0i}. The resonance frequencies are

$$\omega_{0i}^2=\frac{Ne^2}{m_e\alpha_i}\ . \tag{5}$$

Classical electrodynamics relates the α_i to the depolarization factors, D_i,

$$\frac{\alpha_i}{\alpha_j}=\frac{D_j}{D_i}\ . \tag{6}$$

The D_i can easily be calculated[26] if the axial ratios of the ellipsoid are known (see Sec. IV C).

In order to find the absolute values of the α_i, we use the experimental measurement of average static polarizabilities in Na clusters.[16,17] For randomly oriented ellipsoids, the average polarizability, $\bar{\alpha}$, is

$$\bar{\alpha}=\tfrac{1}{3}\sum_{i=1}^{3}\alpha_i\ . \tag{7}$$

Combining Eqs. (6) and (7), and inserting the experimental $\bar{\alpha}$, the α_i are obtained. Equation (5) then gives the three resonance frequencies.

C. Axial ratios and resonance wavelengths

The Clemenger model for metal clusters[14] is based on the Nilsson model for nuclei.[27] It is assumed that the valence electrons can be described as moving in an effective one-electron potential, which is approximated by an anisotropic harmonic oscillator with a small angular-momentum-dependent perturbation. The cluster shapes are restricted to spheres or spheroids, and the equilibrium shapes are determined by minimizing the sum of the one-electron energies. We have extended the Clemenger model to ellipsoids, using a three-dimensional harmonic-oscillator potential with no perturbation term. The latter, which would flatten the bottom of the potential well, is nonessential for small clusters (see below).

For a three-dimensional harmonic potential, the energy eigenvalues are

$$E_{n_x,n_y,n_z}=\hbar\omega_0[(n_x+\tfrac{1}{2})/x_0+(n_y+\tfrac{1}{2})/y_0+(n_z+\tfrac{1}{2})/z_0]\ . \tag{8}$$

$\omega_0 e_x$, $\omega_0 e_y$, and $\omega_0 e_z$ are the oscillator frequencies along the three principal axes of the ellipsoid, which has axial rates x_0, y_0, and z_0, respectively. The parameter ω_0 sets the energy scale, and does not affect the equilibrium shapes. The total energy of the cluster is given by

$$E_{\rm tot}=\hbar\omega_0\left[\frac{C_x}{x_0}+\frac{C_y}{y_0}+\frac{C_z}{z_0}\right]\ , \tag{9}$$

where $C_i=\sum(n_i+\frac{1}{2})$, the sums being over all occupied single-electron states.

For a given cluster size, and for a particular electronic configuration, $E_{\rm tot}$ is minimized with respect to the principal axes, keeping the volume constant. This process is repeated for all possible configurations; the resulting minimum total energy determines the axial ratios for the chosen cluster size.

In some cases, two different electronic configurations of the same cluster (each corresponding to a different set

of axial ratios) give very similar total energies. For a few clusters in the size range $N=2-40$, we estimate that this energy difference is $\lesssim 3k_BT$ (where $T\sim 300$ K; see, for example, Ref. 40), suggesting that cluster-shape isomerism may occur. In a spheroidal self-consistent calculation,[28,29] a similar result is obtained: for both Na_{13} and Na_{21} there are two configurations (corresponding to a prolate or an oblate spheroid, respectively) which are particularly close in energy.

Results of our model for Na_{2-40} are given in Table I. The closed-shell clusters $N=8$, 20, and 40 are predicted to be spherical; the others are either spheroidal or ellipsoidal. For the spheroidal clusters, distortion parameters[30] are given; they are compared to Clemenger's calculations[14,17] and to a self-consistent spheroidal calculation.[28,29] There is good agreement between our model and Clemenger's in the cluster-size range $N=2-40$, demonstrating that omission of the angular-momentum-dependent perturbation term from the Nilsson Hamiltonian does not significantly affect the calculated distortion parameters in small clusters. Our results are also similar to those of Ekardt. We note that agreement be-

TABLE I. Axial ratios of Na_N clusters calculated with the ellipsoidal shell model. Distortion parameters (Ref. 30) are given for those clusters which are found to be spheroidal in shape. For comparison, distortion parameters calculated with the spheroidal models of Clemenger (Refs. 14 and 17) and Ekardt (Refs. 28 and 29) are shown.

	Axial ratios			Distortion parameters		
N	x_0	y_0	z_0	Present ellipsoidal model (see Sec. IV C)	Clemenger	Ekardt
2	1	1	1	0	0	0
3	0.843	0.843	1.406	0.50	0.50	0.61
4	0.794	0.794	1.587	0.67	0.67	0.78
5	0.735	1.029	1.323			
6	0.711	1.186	1.186	−0.50	−0.50	−0.63
7	0.875	1.069	1.069	−0.20	−0.20	−0.27
8	1	1	1	0	0	0
9	0.914	0.914	1.196	0.27	0.25	0.26
10	0.860	0.860	1.352	0.44	0.44	0.48
11	0.809	0.917	1.348			
12	0.770	0.963	1.348			
13	0.736	1.082	1.255			
14	0.711	1.186	1.186	−0.50	−0.49	−0.56
15	0.755	1.115	1.187			
16	0.794	1.058	1.191			
17	0.826	1.070	1.132			
18	0.854	1.082	1.082	−0.24	−0.21	−0.17
19	0.930	1.037	1.037	−0.11	0	0
20	1	1	1	0	0	0
21	0.956	0.956	1.095	0.14	−0.07	0.09(−0.07)
22	0.920	0.920	1.182	0.25	0.21	0.22
23	0.886	0.928	1.216			
24	0.857	0.935	1.247			
25	0.868	0.905	1.274			
26	0.877	0.877	1.299	0.39	0.36	0.37
27	0.850	0.917	1.283			
28	0.826	0.953	1.271			
29	0.833	0.954	1.257			
30	0.783	1.073	1.189			
31	0.792	1.070	1.181			
32	0.800	1.066	1.173			
33	0.807	1.088	1.139			
34	0.813	1.109	1.109	−0.31	−0.23	−0.18
35	0.841	1.102	1.078			
36	0.868	1.051	1.096			
37	0.893	1.047	1.069			
38	0.917	1.045	1.045	−0.13	−0.10	−0.09
39	0.959	1.021	1.021	−0.06	−0.04	−0.05
40	1	1	1	0	0	0

TABLE II. Experimental per-atom static electric polarizabilities for Na_N clusters (Refs. 16 and 17), normalized to the measured polarizability of the Na atom (Ref. 31). The corresponding surface-plasma-resonance wavelengths $\lambda_x, \lambda_y, \lambda_z$ of ellipsoidal clusters (with axial ratios as given in Table I) are also shown.

N	Experimental polarizability	Resonance wavelengths (nm) λ_x	λ_y	λ_z
2	0.803	515	515	515
3	0.986	501	501	691
4	0.857	439	439	681
5	0.911	448	544	638
6	0.862	428	580	580
7	0.727	452	509	509
8	0.691	478	478	478
9	0.739	465	465	549
10	0.814	464	464	614
11	0.743	428	460	585
12	0.782	426	485	599
13	0.742	406	509	559
14	0.748	399	540	540
15	0.733	412	517	539
16	0.760	433	512	552
17	0.674	419	488	506
18	0.654	422	485	485
19	0.669	451	480	480
20	0.652	464	464	464
21	0.625	442	442	479
24	0.653	419	440	527
25	0.634	415	425	525
26	0.658	424	424	542
30	0.612	385	463	494
34	0.632	401	483	483
40	0.630	456	456	456
classical sphere	0.402	365	365	365

tween our calculated photoabsorption spectra and the experimental results depends sensitively on the predicted resonance positions, which are directly related to the calculated distortion parameters (see above).

Saunders[15] has extended the Clemenger model to ellipsoids, while retaining the perturbation term in the Hamiltonian. This term is shell dependent—its value is chosen to give the best agreement with experimental abundance spectra and photoionization thresholds. Results of this calculation differ only slightly with respect to ours.

The calculated axial ratios, together with the experimental static polarizabilities, are used to obtain the surface-plasma-resonance frequencies of each cluster. The corresponding resonance wavelengths are given in Table II, for those clusters for which the experimental polarizabilities[16,17] are known. The latter are also shown, normalized to the measured value for the Na atom.[31]

V. COMPARISON OF EXPERIMENT AND THEORY

Figure 6 shows the measured per-atom photoabsorption cross sections versus wavelength for several selected clusters in the wavelength range of 452–604 nm, along with predictions of our model from Sec. IV. The damping constant Γ is chosen as $0.15\omega_0$. The model predicts that Na_8 and Na_{20} are spherical. Na_9 and Na_{10} are expected to be prolate spheroids, while Na_{12} is ellipsoidal.

In Fig. 7 the measured and theoretical photoabsorption cross sections are shown as a function of cluster size for Na_{3-21} at two selected wavelengths. Near 600 nm the cross sections of the open-shell clusters are strongly enhanced with respect to those of the spherical closed-shell clusters. However, near 500 nm the closed-shell cross sections are the larger. The measured photoabsorption cross sections for Na_{22-40} are also consistent with the model.[1] The cross section of the dimer is uniquely very small or zero at all investigated wavelengths. It is known that Na_2 absorbs visible light,[7] but most of the energy is reradiated, and so we do not observe beam depletion. The fluorescence is so strong that optical pumping of Na_2 can produce laser emission.[32]

The self-consistent jellium model in the time-dependent local-density approximation has been used to calculate

photoabsorption spectra of spherical metal clusters.[24,33] The spectrum contains the surface plasma resonance and several single-particle resonances. Landau damping (the decay of the surface plasma oscillations via excitation of single electron-hole pairs) contributes to the surface-plasma-resonance width.[24] For Na_8, the calculated surface-plasma-resonance position[33] is red-shifted by 19% with respect to the classical value; our data indicate a red shift of about 25%. We have not yet identified any single-particle resonances.

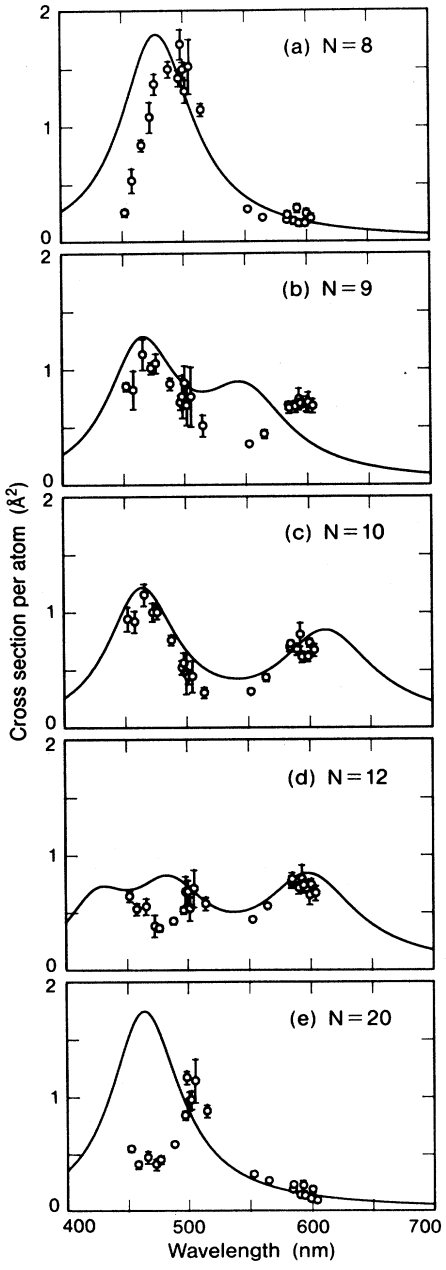

FIG. 6. Experimental (circles) and theoretical (solid lines) photoabsorption cross sections vs wavelength for (a) Na_8, (b) Na_9, (c) Na_{10}, (d) Na_{12}, and (e) Na_{20}. For the theoretical curves, the widths are $\Gamma=0.15\omega_0$.

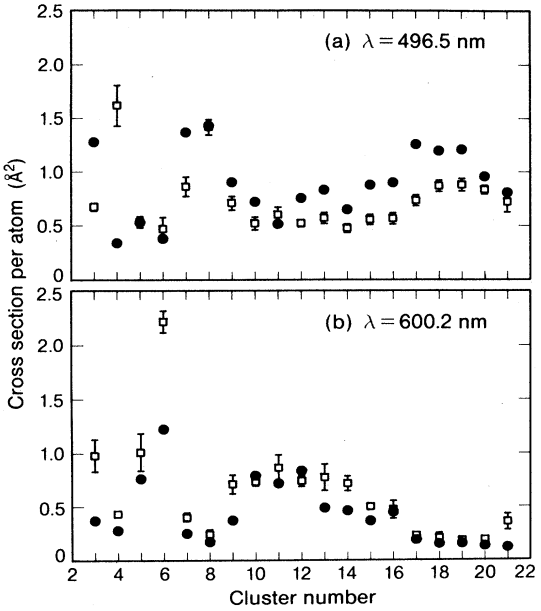

FIG. 7. Experimental (squares) and theoretical (circles) photoabsorption cross sections vs cluster size, at wavelengths of (a) 496.5 nm and (b) 600.2 nm, for Na_{3-21}. The theoretical cross sections are calculated using $\Gamma=0.15\omega_0$.

Brack[34] has used random-phase-approximation (RPA) sum-rule techniques to calculate the eigenmode spectrum for collective electronic excitations of spherical metal clusters. For the static polarizabilities and the surface-plasma-resonance frequencies, good agreement is obtained with the calculations of Ekardt[24] and Beck.[33,35] An estimate of the surface-plasma-resonance width is consistent with experiment.

The Thomas-Fermi statistical method has been used with the RPA to calculate the surface-plasma-resonance frequencies of spherical metal clusters;[36] the value for Na_8 is in good agreement with our data. These resonance positions are used to deduce the static electric polarizabilities, which agree well with experiment.[16,17] It is important to take into account correctly the spillout of the valence electrons outside the boundary of the positive ions in the cluster. This spillout causes an enhanced static electric polarizability, and a red shift of the surface plasma resonance, with respect to the bulk values (see Table III).

In Sec. IV the experimental static polarizabilities of Na clusters[16,17] were used to deduce the surface-plasma-resonance frequencies [Eq. (3)]. The experimental resonance position for the closed-shell cluster Na_8 is in good agreement with our calculated value [see Fig. 6(a) and Table III].

Table III shows the experimental resonance wavelengths for the spherical clusters Na_8 and Na_{20} (for Na_{20} more data are needed to define accurately the resonance position). The resonance wavelengths deduced from the

TABLE III. Experimental surface-plasma-resonance wavelengths of Na_8 and Na_{20}. The resonance wavelengths deduced from the experimental polarizabilities (Refs. 16 and 17; see also Table II) are also shown. For comparison, some theoretical results are given (Refs. 24, 33, and 36).

	Resonance wavelength (nm)	
	Na_8	Na_{20}
Experiment	495±5	505±10
From experimental static electric polarizability	478±4	464±13
Ekardt		412
Beck	452	461
Kresin	493	462
Classical metal sphere (r_s=4.0 a.u.)	365	365

experimental static polarizabilities are given, together with the values calculated from the time-dependent jellium model,[24,33] and the Thomas-Fermi statistical method.[36] All these calculations, and also the data, give surface-plasma-resonance positions which are substantially red-shifted with respect to the value for a classical metal sphere (365 nm). This is due to the spillout of the valence electrons. Larger free Na clusters of radii $R \sim 7$ nm (Ref. 5) show a surface-plasma-resonance peak at 384 nm, demonstrating that the relative effect of the electron spillout decreases with increasing cluster size, causing the resonance peak to move towards the classical value.

Although we do not yet have sufficient data to determine the resonance widths, $\Gamma \sim 0.15\omega_0$ is consistent with experiment for all investigated clusters. Some other experiments and calculations that suggest possible damping mechanisms for small Na clusters are discussed below.

Numerous experimental data are available for the plasma resonance widths of bulk surfaces;[37] it is interesting to compare these results with the measurements of surface plasmon widths of clusters.[4] However, prior to the present work, few data existed either for free clusters, or for clusters with radii $R \lesssim 1$ nm. To date, most of the relevant observations refer to clusters in thin films or embedded in matrices; the observed widths are mainly in the range 0.1–1.0 eV. For embedded metal particles in the size range 1–10 nm, the experimental surface plasmon width varies inversely with the cluster radius.[4,38] However, for free Na particles, our experimental width for Na_8 differs by less than 20% from that observed for clusters with $R \sim 7$ nm.[5] This result is inconsistent with a $1/R$ dependence of the width, suggesting that this relationship is not applicable to the very small clusters in our experiment.

Calculations of the damping due to coupling of surface plasma oscillations to quadrupole shape fluctuations of the cluster have recently been presented.[39,40] This contribution is temperature dependent, but does not vary dramatically with cluster size. The damping factor at room temperature is found to be $0.07\omega_0 < \Gamma < 0.14\omega_0$ for clusters in the size range $N = 8-20$.[40]

The spherical jellium model with the RPA has been used to calculate the photoabsorption spectra of spherical metal clusters;[22] Landau damping and exchange and correlation effects are found to be important. When the damping due to coupling with surface vibrations[40] is included in these spectra, the resulting line shapes conform to the experimental data. For Na_8, the authors find a single peak in the collective dipole spectrum at 2.8 eV, which exhausts 75% of the dipole oscillator strength. For Na_{20}, they find the same strength distributed in two closely spaced peaks at 2.6 and 2.9 eV. The experimental data for Na_{20} suggest the possibility of a double peak, but further measurements are required to verify it.

The observed giant dipole resonances in nuclei,[41], which can be described as the collective motion of the protons with respect to the neutrons, show many similarities to surface plasma resonances in metal clusters. These nuclear resonances show single (spherical) or double (spheroidal) peaks, and are seen in nuclei as small as ^{4}He. Single-nucleon excitations give rise to sharp peaks superimposed on the giant dipole resonance profile. It is therefore reasonable to expect both single-particle and collective behavior in metal clusters, including small ones such as the trimer. Studies of the damping of nuclear giant dipole resonances find that Landau damping and coupling to nuclear shape oscillations are important,[42] giving support to the predictions that these damping mechanisms exist in clusters. For small nuclei, the escape of particles into the continuum provides a major contribution to the width of the giant resonance.[42] This mechanism is less important for heavy nuclei, where it produces about 15% of the total width.

The decay of cluster surface plasma oscillations into thermal motion is one of several steps in the beam depletion process for our experiment. There is evidence that depletion is completed in times much shorter than the cluster time of flight (see Sec. III), but the details of the process are not known, and there are currently no other experimental data available giving a time scale for plasmon decay in small metal clusters. However, for noble-metal films, there is evidence for surface plasmon decay and related heating in times as short as 50 fs,[43] and for electron-phonon energy transfers on a picosecond timescale.[44]

VI. CONCLUSIONS

For clusters with $N \gtrsim 3$, our data are generally consistent with a sum-rule calculation based on an ellipsodial shell model and the experimental static polarizabilities of Na clusters. Na_8 shows a single peak, as expected for spheres; Na_9 and Na_{10} show spectra consistent with the expected prolate spheroid cluster shape. Triple peaks for Na_{11}, Na_{12}, and Na_{13} have not been resolved, but the relatively flat spectra do not show the stronger peaks typical of spherical or spheroidal clusters. The observed peak for Na_{20} is somewhat red-shifted from our prediction, and it does not exhaust the dipole sum rule. It is possible that we have observed one of two closely spaced peaks in

the photoabsorption spectrum.

For all clusters in the size range $N=3-40$, the observed cross sections for a given cluster size average to about 1 $Å^2$ per delocalized electron. However, as mentioned earlier, our data indicate that the cross sections for Na_2 are substantially smaller.

For many of the investigated cluster sizes, the measured photoabsorption spectra show multipeak structure consistent with the ellipsoidal shell model, showing that this model is a reasonable first approximation. However, as we have noted, there are significant deviations for some clusters. In continuing studies, cluster photoabsorption cross sections will be measured at many other wavelengths, and the peak positions, widths, and strengths of the surface plasma resonances will be determined. Deviations from the predictions of the ellipsoidal shell model should indicate the relative importance of ellipsoidal distortions, single-particle versus collective electron dynamics, and the basic electron-electron interactions in metal clusters.

ACKNOWLEDGMENTS

This work is supported by the U.S. National Science Foundation under Grant No. DMR-86-15246. We thank A. Châtelain and M. Kruger for their participation in the experiment. We have benefited greatly from discussions with M. L. Cohen, S. G. Louie, S. Saito, V. Z. Kresin, W. Ekardt, and Z. Penzar. We are grateful to E. Commins, A. Kung, and T. Hadeishi for the loan of lasers. We thank G. F. Bertsch, D. Tománek, C. Yannouleas, J. Pacheco, and M. Brack for sending preprints of their recent work. One of us (M.V.) acknowledges the support of the Deutsche Forschungsgemeinschaft (Bonn, Germany).

APPENDIX A: THE EVAPORATION RATE OF ATOMS

We will assume that the energy of an absorbed photon decays into thermal motion, leading to a rise in the cluster temperature. In order to estimate a lower limit on the evaporation rate of atoms (we will not consider evaporation of dimers) from neutral sodium clusters, we first consider the temperature rise, ΔT, of an N-atom cluster, after absorption of a photon of energy E. An N-particle system has $3N-6$ vibrational modes; thus we obtain

$$\Delta T=\frac{E}{(3N-6)k_B} . \tag{A1}$$

Clusters larger than the tetramer do not appear in saturated alkali vapors;[45] they evaporate atoms at a rate faster than they grow. Assuming a sticking coefficient of 1, kinetic gas theory gives an expression for the growth rate,[46] which we will consider to be a lower limit on the evaporation rate, R:

$$R=\frac{Ap(T)}{(2\pi mk_BT)^{1/2}} \text{ atoms/s} , \tag{A2}$$

where A is the cluster surface area, T is the cluster temperature, $p(T)$ is the vapor pressure of Na at temperature T, and m is the mass of the atoms. The average time for evaporation of an atom is $\tau=1/R$.

TABLE IV. Estimated average times, τ, for evaporation of an atom from Na_N clusters, after absorption of a 500 nm photon. The cluster temperature before photoabsorption is assumed to be 200 K.

N	τ (s)
10	4×10^{-11}
20	6×10^{-8}
30	1×10^{-5}
40	1×10^{-3}

The temperature increases calculated from Eq. (A1) are inserted into Eq. (A2), with $A=4\pi N^{2/3}r_s^2$ (and $r_s=4.0$ a.u.), together with the vapor pressures of bulk Na.[47] In Table IV, Eq. (A2) is evaluated for selected Na clusters. The initial cluster temperature is assumed to be 200 K, which is an estimated lower limit of the cluster temperatures in our apparatus. For $N\lesssim30$ the calculated evaporation times, τ, are much shorter than the cluster flight time ($\sim10^{-3}$ s). The evaporation time increases rapidly with cluster size and, for $N=40$, τ is of the same order as the flight time.

However, this result does not imply that our model for the beam depletion mechanism breaks down for $N>40$, as our calculation is expected to give values of τ which are much larger than they are in reality. Firstly, Eq. (A2) is actually the *growth* rate of the cluster in saturated vapor, which is known to be smaller than the evaporation rate (see above). Moreover, bulk vapor pressures were used in Eq. (A2) to obtain the evaporation rates; in fact, the vapor pressure of small particles increases rapidly with decreasing size.[48] The true evaporation times for clusters are therefore expected to be much shorter than the values given in Table IV.

APPENDIX B: DETECTION PROBABILITY OF DAUGHTER CLUSTERS

We will demonstrate that the detection probability of daughter clusters is negligible, unless evaporation occurs when the parent cluster is very close to the detector aperture. Consider an N-atom cluster moving with velocity u towards the detector; the cluster absorbs a photon and subsequently evaporates an atom of mass m. We will neglect the time delay between photon absorption and evaporation, as it is much shorter than the cluster flight time (see Appendix A).

In the center of mass frame the process is isotropic, and the atom and the daughter cluster [of mass $M=(N-1)m$] have equal and opposite momenta. Let the kinetic energy of the evaporated atom be $\frac{3}{2}k_BT$; then the velocity, v_d, of the daughter cluster is

$$v_d=(1/M)(3mk_BT)^{1/2} , \tag{B1}$$

where T is the temperature of the parent cluster at the time of evaporation. Let the evaporation occur at a time $t=0$, when the cluster is a distance L from the detector aperture, which we will assume to be circular with radius r. Let the angle of the velocity of the daughter cluster

with respect to the beam axis be θ.

In the laboratory frame, the velocity component of the daughter cluster along the beam axis is given by

$$v = u + v_d \cos\theta \ . \tag{B2}$$

The daughter crosses the plane of the detector aperture at time $t = L/v$, having traveled a transverse distance $y = v_d t \sin\theta$. It will be detected if $y < r$; this condition corresponds to angles $\theta < \theta_m$, where θ_m is given by

$$\sin\theta_m = \frac{r}{L}\left[\frac{u}{v_d} + \cos\theta_m\right] \ . \tag{B3}$$

This equation has two relevant solutions: θ_{m1} and θ_{m2} (where θ_{m2} corresponds to backscattered fragments).

All values of θ (in the range $0-\pi$) are equally probable, and the detection probability of the daughter cluster, $P_{\rm det}$, is the total probability that $0 < \theta < \theta_{m1}$ or $\theta_{m2} < \theta < \pi$:

$$P_{\rm det} = 1 - \tfrac{1}{2}(\cos\theta_{m1} - \cos\theta_{m2}) \ . \tag{B4}$$

After some algebra, one obtains

$$P_{\rm det} = 1 - \cos\theta_d \left[1 - \left[\frac{u}{v_d}\sin\theta_d\right]^2\right]^{1/2} , \tag{B5}$$

where $\tan\theta_d = r/L$.

For $L \lesssim r$, $P_{\rm det}$ is unity: evaporation occurs so close to the detector aperture that even daughters with $\theta = \pi/2$ enter it. $P_{\rm det}$ decreases rapidly as L increases, because the daughter clusters travel greater transverse distances before crossing the plane of the aperture. We now evaluate Eq. (B5) for typical experimental conditions (see Fig. 2). Consider Na_8 clusters with $u = 1.1 \times 10^3$ m/s, and let $r = 0.15$ cm, an approximation of our 2×3 mm^2 rectangular detector aperture. We use $T = 1750$ K, which is calculated from Eq. (A1), assuming a photon wavelength of 514.5 nm and a cluster temperature before photoabsorption of 200 K. The results are shown in Table V.

TABLE V. Calculated detection probability, $P_{\rm det}$, for Na_8 clusters which absorb a 514.5-nm photon and evaporate an atom at a distance L from the detector aperture.

L (cm)	$P_{\rm det}$ (%)
1.0	100
2.0	20
3.0	7
5.0	3
10.0	0.6
20.0	0.2
30.0	0.07

The short laser pulses (1 μs width) used for Fig. 2 greatly simplify understanding of the signal shape, because the clusters move a negligible distance during each pulse. A more sophisticated calculation would incorporate the initial velocity distribution of the clusters, and the energy distribution of the evaporated atoms.

*Permanent address: Physikalisches Institut der Universität Heidelberg, D-6900 Heidelberg 1, Federal Republic of Germany.

†Permanent address: Department of Physics, Cornell University, Ithaca, NY 14853.

‡Permanent address: Institut de Physique Expérimentale, Ecole Polytechnique Fédérale de Lausanne, PHB-Ecublens, CH-1015 Lausanne, Switzerland.

[1]W. A. de Heer, K. Selby, V. Kresin, J. Masui, M. Vollmer, A. Châtelain, and W. D. Knight, Phys. Rev. Lett. **59**, 1805 (1987).

[2]K. Selby, M. Vollmer, J. Masui, V. Kresin, W. A. de Heer, and W. D. Knight, Z. Phys. D (to be published).

[3]J. A. A. J. Perenboom, P. Wyder, and F. Meier, Phys. Rep. **78**, 173 (1981).

[4]U. Kreibig and L. Genzel, Surf. Sci. **156**, 678 (1985).

[5]D. M. Mann and H. P. Broida, J. Appl. Phys. **44**, 4950 (1973).

[6]J. Hecht, J. Appl. Phys. **50**, 7186 (1979).

[7]W. Demtröder, M. McClintock, and R. N. Zare, J. Chem. Phys. **51**, 5495 (1969).

[8]J. L. Gole, G. J. Green, S. A. Pace, and D. R. Preuss, J. Chem. Phys. **76**, 2247 (1982).

[9]M. Broyer, G. Delacrétaz, G.-Q. Ni, R. L. Whetten, J.-P. Wolf, and L. Wöste, J. Chem. Phys. **90**, 843 (1989).

[10]W. A. de Heer, W. D. Knight, M. Y. Chou, and M. L. Cohen, in *Solid State Physics,* edited by F. Seitz and D. Turnbull (Academic, New York, 1987), Vol. 40, p. 93.

[11]C. L. Pettiette, S. H. Yang, M. J. Craycraft, J. Conceicao, R. T. Laaksonen, O. Cheshnovsky, and R. E. Smalley, J. Chem. Phys. **88**, 5377 (1988).

[12]G. Ganteför, M. Gausa, K. H. Meiwes-Broer, and H. O. Lutz, Z. Phys. D **9**, 253 (1988).

[13]K. H. Bowen, Z. Phys. D (to be published).

[14]K. Clemenger, Phys. Rev. B **32**, 1359 (1985).

[15]W. A. Saunders (unpublished).

[16]W. D. Knight, K. Clemenger, W. A. de Heer, and W. A. Saunders, Phys. Rev. B **31**, 2539 (1985).

[17]K. Clemenger, Ph.D. thesis, University of California, Berkeley, 1985.

[18]W. A. Saunders, Ph.D. thesis, University of California, Berkeley, 1986.

[19]M. Vollmer, K. Selby, V. Kresin, J. Masui, M. Kruger, and W. D. Knight, Rev. Sci. Instrum. **59**, 1965 (1988).

[20]C. Bréchignac, Ph. Cahuzac, J. Leygnier, R. Pflaum, J.-Ph. Roux, and J. Weiner, Z. Phys. D (to be published).

[21]W. Hoheisel, K. Jungmann, M. Vollmer, R. Weidenauer, and F. Träger, Phys. Rev. Lett. **60**, 1649 (1988); W. Hoheisel, U. Schulte, M. Vollmer, R. Weidenauer, and F. Träger, Appl. Surf. Sci. **36**, 644 (1989).

[22]C. Yannouleas, M. Brack, R. A. Broglia, and P. F. Bortignon, Phys. Rev. Lett., July (1989).

[23]G. Mie, Ann. Phys. (Leipzig) **25**, 377 (1908).

[24]W. Ekardt, Phys. Rev. B **31**, 6360 (1985).

[25]A. A. Lushnikov, V. V. Maksimenko, and A. J. Simonov, in *Electromagnetic Surface Modes,* edited by A. D. Boardman (Wiley, New York, 1982).

[26]E. C. Stoner, Philos. Mag. **36**, 803 (1945).

[27]S. G. Nilsson, Det. Kong. Dan. Vidensk. Selsk. Mat.-Fys. Medd. **29**, No. 16 (1955).

[28]W. Ekardt and Z. Penzar, Phys. Rev. B **38**, 4273 (1988).

[29]We are grateful to W. Ekardt and Z. Penzar for giving us new results of their self-consistent spheroidal jellium model calculation prior to publication.

[30]For a spheroidal cluster, the distortion parameter δ is defined as $\delta=2(Z_0-\rho_0)/(Z_0+\rho_0)$, where Z_0 is the length of the symmetry axis and ρ_0 is the length of the perpendicular axes of the ellipsoid (Ref. 14).

[31]R. W. Molof, H. L. Schwartz, T. M. Miller, and B. Bederson, Phys. Rev. A **10**, 1131 (1974).

[32]M. A. Henesian, R. L. Herbst, and R. L. Byer, J. Appl. Phys. **47**, 1515 (1976).

[33]D. E. Beck, Phys. Rev. B **35**, 7325 (1987).

[34]M. Brack, Phys. Rev. B **39**, 3533 (1989).

[35]D. E. Beck, Phys. Rev. B **30**, 6935 (1984).

[36]V. Kresin, Phys. Lett. A **133**, 89 (1988); V. Kresin, Phys. Rev. B **39**, 3042 (1989).

[37]H. Raether, *Excitation of Plasmons and Interband Transitions by Electrons* (Springer, New York, 1980).

[38]M. A. Smithard, Solid State Commun. **14**, 407 (1974).

[39]G. F. Bertsch and D. Tománek, Phys. Rev. B **40**, 2749 (1989).

[40]J. M. Pacheco and R. A. Broglia, Phys. Rev. Lett. **62**, 1400 (1989).

[41]B. L. Berman and S. C. Fultz, Rev. Mod. Phys. **47**, 713 (1975).

[42]G. F. Bertsch, P. F. Bortignon, and R. A. Broglia, Rev. Mod. Phys. **55**, 287 (1983).

[43]M. van Exter and A. Lagendijk, Phys. Rev. Lett. **60**, 49 (1988).

[44]H. E. Elsayed-Ali, T. B. Norris, M. A. Pessot, and G. A. Mourou, Phys. Rev. Lett. **58**, 1212 (1987).

[45]C. T. Ewing, J. P. Stone, J. R. Spann, and R. R. Miller, J. Phys. Chem. **71**, 473 (1967).

[46]F. Reif, *Fundamentals of Statistical and Thermal Physics* (McGraw-Hill, New York, 1965).

[47]*CRC Handbook of Chemistry and Physics,* 50th ed., edited by R. C. Weast (Chemical Rubber Co., Cleveland, 1969).

[48]J. R. Sambles, L. M. Skinner, and N. D. Lisgarten, Proc. R. Soc. London, Ser. A **318**, 507 (1970).